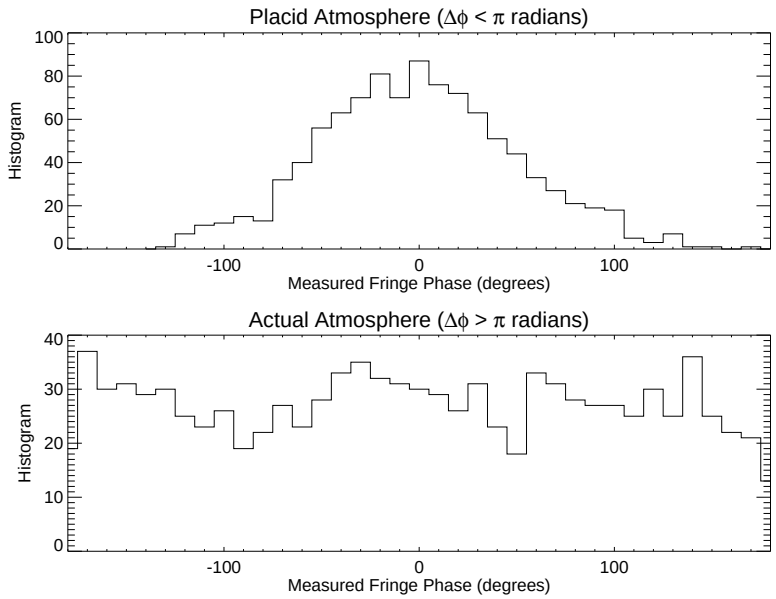

Figure 13.2: *Top Panel:* A simulation of measured fringe phases when the atmosphere induces small phase shifts. The intrinsic phase (0 degrees) could be extracted from such a dataset. *Bottom Panel:* A simulation of measured fringe phases for a turbulent atmosphere which causes phase shifts greater than π radians. All phase information is lost.

13.1.2 Phase Referencing

In Chapter 9 of this volume, possible techniques for recovering this phase information using *phase referencing* are described. I will briefly mention only three of these.

1. **Nearby Sources.** If a bright point source (or source with well-known structure) lies within an isoplanatic patch (see Chapter 5), then its fringes will act as a probe of the atmospheric conditions. By measuring the instantaneous phases of fringes from the bright source, one can correct the corrupted phases on the science target. This has been applied to narrow-angle astrometry where fringe-phase information is used for determining precise relative positions of nearby stars (Shao and Colavita 1992; Colavita *et al.* 1999). While it would be very valuable to use an artificial guide star for phase referencing a long baseline interferometer, current laser beacons are too spatially extended; schemes exist to circumvent this problem (Gavel *et al.* 1998).

2. **Measuring $\Delta\Phi$.** In the millimeter and sub-millimeter bands, phase shifts caused by fluctuations in the column density of atmospheric water-vapour can be monitored by observing its line emission. This information can be used to phase-compensate the interferometer, allowing longer coherent integrations and accurate fringe-phase determination on the target (Wiedner 1998, and references therein). In the mid-infrared, strategies to actively monitor ground-level turbulence using temperature

sensors are being explored by the Infrared Spatial Interferometry group at Mt. Wilson motivated by recent atmospheric studies (e.g., Bester *et al.* 1992).

3. **Spectral Lines.** Another possibility is to observe a target at multiple wavelengths and to use data from one part of the spectrum to calibrate another. For example, one might use fringes formed by the continuum emission to phase reference a spectral line (e.g., Vakili *et al.* 1997).

Phase referencing is not feasible for most sources, and one must make use of *closure quantities*.

13.2 The Closure Quantities

13.2.1 Closure Phase and the Bispectrum

Consider Figure 13.3 in which a phase delay is introduced above telescope 2. This causes a phase shift in the fringe detected between telescopes 1–2, as discussed in the last section. Note that a phase shift is also induced for fringes between telescopes 2–3; however, this phase shift is equal but *opposite* to the one for telescopes 1–2.

$$\begin{array}{rcl} \text{Observed} & & \text{Intrinsic} \quad \text{Atmosphere} \\ \Phi(1{-}2) & = & \Phi_0(1{-}2) + [\phi(2) - \phi(1)], \qquad (13.6) \\ \Phi(2{-}3) & = & \Phi_0(2{-}3) + [\phi(3) - \phi(2)], \qquad (13.7) \\ \Phi(3{-}1) & = & \Phi_0(3{-}1) + [\phi(1) - \phi(3)]. \qquad (13.8) \end{array}$$

Hence, the sum of three fringe phases, between 1–2, 2–3, and 3–1, is insensitive to the phase delay above telescope 2.

$$\begin{array}{rcl} \text{Closure Phase}\,(1{-}2{-}3) & = & \Phi(1{-}2) + \Phi(2{-}3) + \Phi(3{-}1) \\ & = & \Phi_0(1{-}2) + \Phi_0(2{-}3) + \Phi_0(3{-}1). \qquad (13.9) \end{array}$$

This argument holds for arbitrary phase delays above any of the three telescopes. In general, the sum of three phases around a closed triangle of baselines, the *closure phase*, is a good interferometric observable; that is, it is independent of telescope-specific phase shifts induced by the atmosphere or optics.

The idea of closure phase was first introduced by Jennison to compensate for poor phase stability in early radio VLBI work (Jennison 1958). Although Jennison also described an optical counterpart (Jennison, 1961), Rogstad (1968) is usually credited with first suggesting closure phase techniques at optical wavelengths. The first experiments at optical telescopes, using aperture masks, were only carried out some twenty years later (Baldwin *et al.* 1986; Haniff *et al.* 1987; Readhead *et al.* 1988; Haniff *et al.* 1989). Currently only two separate-element interferometers have succeeded in obtaining closure-phase measurements, in the

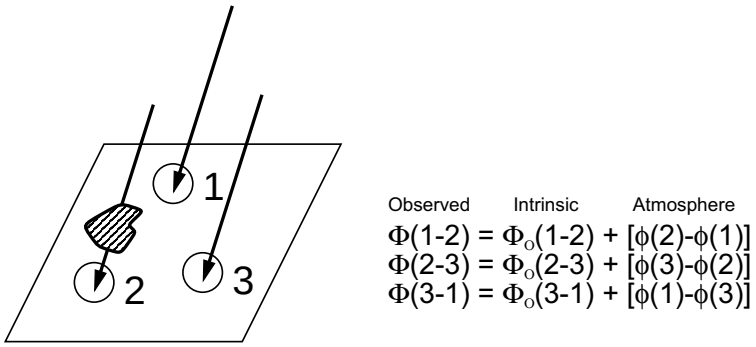

Figure 13.3: Phase errors introduced at any telescope in an array causes equal but opposite phase shifts, canceling out in the *closure phase*, which is the sum of $\Phi(1–2)$, $\Phi(2-3)$, and $\Phi(3-1)$ (see Readhead *et al.* 1988).

optical/infrared, first at COAST (Baldwin *et al.* 1996) and soon after at NPOI (Benson *et al.* 1997).

Another way to derive the invariance of the closure phase to telescope-specific phase shifts is through the *bispectrum*. The bispectrum $\tilde{B}_{ijk} = \tilde{\mathcal{V}}_{ij}\tilde{\mathcal{V}}_{jk}\tilde{\mathcal{V}}_{ki}$ is formed through triple products of the complex visibilities around a closed triangle, where ijk specifies the three telescopes. Using Equation 13.5, we can see how the telescope-specific errors affect the measured bispectrum:

$$\begin{aligned}
\tilde{B}_{ijk} &= \tilde{\mathcal{V}}_{ij}^{\rm measured}\,\tilde{\mathcal{V}}_{jk}^{\rm measured}\,\tilde{\mathcal{V}}_{ki}^{\rm measured} && (13.10)\\
&= |G_i||G_j|\,e^{i(\Phi_i^G-\Phi_j^G)}\,\tilde{\mathcal{V}}_{ij}^{\rm true}\cdot|G_j||G_k|\,e^{i(\Phi_j^G-\Phi_k^G)}\,\tilde{\mathcal{V}}_{jk}^{\rm true}\cdot|G_k||G_i|\,e^{i(\Phi_k^G-\Phi_i^G)}\,\tilde{\mathcal{V}}_{ki}^{\rm true} && (13.11)\\
&= |G_i|^2\,|G_j|^2\,|G_k|^2\,\tilde{\mathcal{V}}_{ij}^{\rm true}\cdot\tilde{\mathcal{V}}_{jk}^{\rm true}\cdot\tilde{\mathcal{V}}_{ki}^{\rm true}. && (13.12)
\end{aligned}$$

From the above derivation, one can see the bispectrum is a complex quantity, and that the phase is identical to the closure phase. The use of the bispectrum for reconstructing diffraction-limited images was developed independently (Weigelt 1977) of the closure-phase techniques, and the connection between the approaches realized only later (Roddier 1986).

13.2.2 Closure Amplitudes

When one has four or more telescopes, another important closure quantity can be formed, the *closure amplitude*. The closure amplitude is constructed to be independent of the telescope-specific gain amplitudes. The closure amplitude A_{ijkl} can be defined in a variety of ways, but here it is defined in terms of four telescopes $ijkl$:

$$A_{ijkl} = \frac{|\tilde{\mathcal{V}}_{ij}^{\rm measured}||\tilde{\mathcal{V}}_{kl}^{\rm measured}|}{|\tilde{\mathcal{V}}_{ik}^{\rm measured}||\tilde{\mathcal{V}}_{jl}^{\rm measured}|} \tag{13.13}$$

$$= \frac{|\tilde{G}_i||\tilde{G}_j||\tilde{\mathcal{V}}_{ij}^{\rm true}||\tilde{G}_k||\tilde{G}_l||\tilde{\mathcal{V}}_{kl}^{\rm true}|}{|\tilde{G}_i||\tilde{G}_k||\tilde{\mathcal{V}}_{ik}^{\rm true}||\tilde{G}_j||\tilde{G}_l||\tilde{\mathcal{V}}_{jl}^{\rm true}|} \tag{13.14}$$

$$= \frac{|\tilde{\mathcal{V}}_{ij}^{\rm true}||\tilde{\mathcal{V}}_{kl}^{\rm true}|}{|\tilde{\mathcal{V}}_{ik}^{\rm true}||\tilde{\mathcal{V}}_{jl}^{\rm true}|}. \tag{13.15}$$

In radio interferometry, this is an important quantity and can be used to compensate for detector gain fluctuations and changing antenna efficiencies. However in the optical and infrared regime, varying fringe amplitudes are not caused by telescope-specific gain changes (such as scintillation), but rather arise from baseline-dependent decorrelation effects related to atmospheric turbulence. Hence, the closure amplitude is not very important to consider for optical/IR interferometers, although recent advances, such as the use of high-order adaptive optics systems and fast fringe tracking, may make this quantity more interesting in the future.

13.2.3 Measuring Closure Phases

Before we discuss how to interpret the closure phases, let us first discuss the appropriate way of measuring them.

Averaging in the Complex Plane

Under noisy conditions, each individual closure-phase measurement may vary from $-180°$ to $180°$. Obviously, averaging the scalar phase in such a case will be useless as shown in Section 13.1.1. However, there is a crucial difference between averaging the closure phases and averaging the fringe phases, and this is illustrated in Figure 13.4. The source of the phase variations in the latter case was atmospheric phase shifts, or "phase noise." However, the closure phase can be thought of as the phase of the bispectrum, and the noise (from detector or Poisson statistics) is an "additive noise." In the left panel of Figure 13.4, the measured bispectrum (thick, solid arrow) is shown in the complex plane and is the sum of a (small) "true" signal (thin, solid arrow) and a larger "noise" vector (dashed arrow). The resulting vector (bispectrum measurement) could lie anywhere on the dashed circle; since the closure phase is the phase of the complex bispectrum, one can see that the closure phase is hardly constrained. However, the right panel shows why averaging of the bispectrum is effective, unlike averaging of the fringe phasors in Section 13.1.1. The "true signal" component of the vector-averaged bispectrum increases linearly with the number of samples N, while the "noise signal" is undergoing a random walk whose rms amplitude grows like $\sqrt{N}$. Simply speaking, the signal-to-noise ratio of the bispectrum measurement should grow like $\sqrt{N}$. Methods of averaging noisy closure phases are discussed in Woan and Duffett-Smith (1988). More detailed (and accurate) analyses of the bispectrum under a wider range of signal-to-

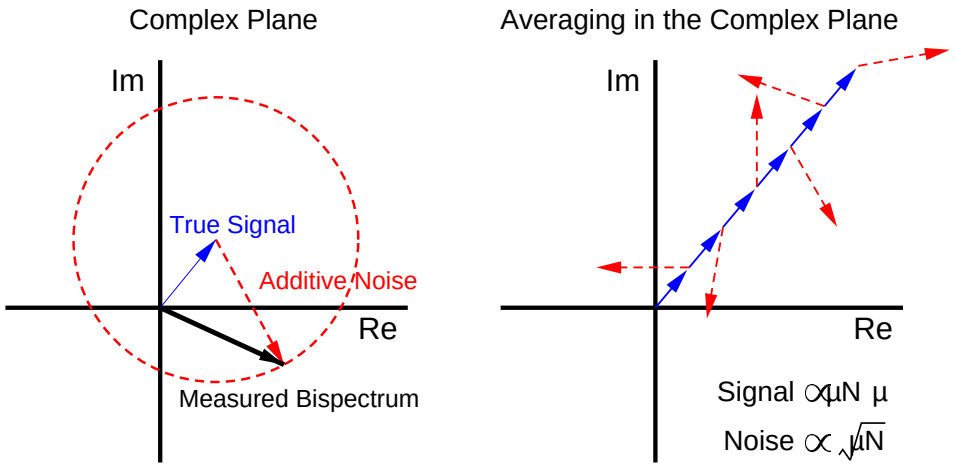

Figure 13.4: The bispectrum is a good observable for optical interferometry. The measured bispectrum is a complex quantity composed of the *true signal* and noise. Vector averaging allows the signal to grow linearly with the number of independent data points N, while the amplitude of the noise term will only grow by $\sqrt{N}$.

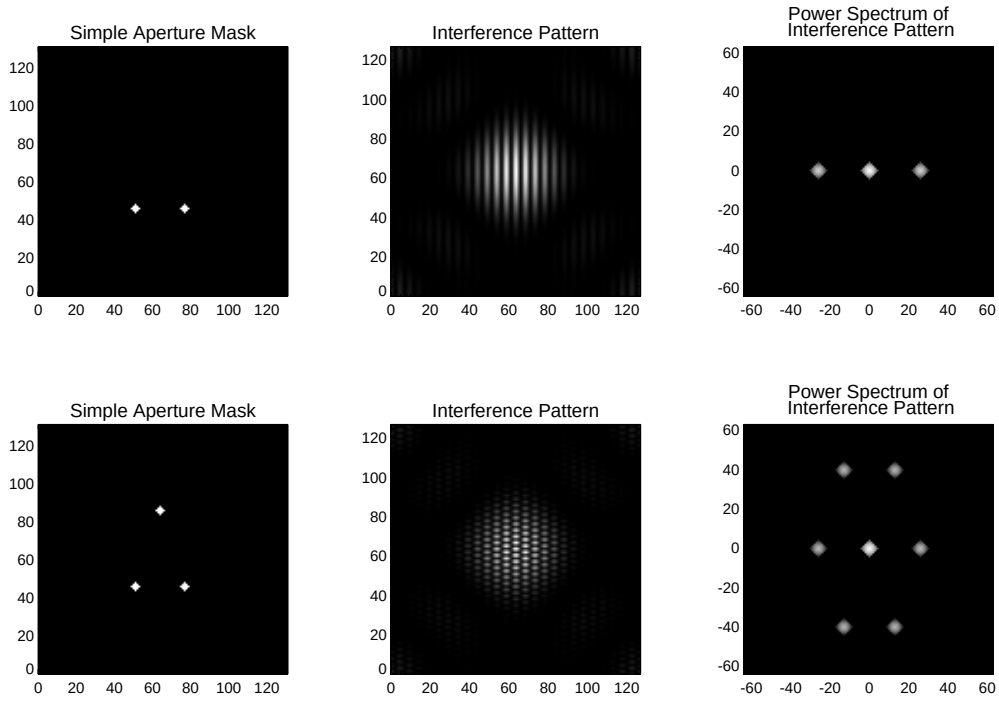

Figure 13.5: The principles of aperture masking. The left panels show the aperture masks being used, while the middle panels show the resulting interference patterns. The right panels result from taking the 2-D power spectra (modulus-squared of 2-D Fourier transform) of the image interference patterns. Each individual fringe pattern becomes a pair of isolated spots in the Fourier plane.

noise conditions are discussed in Readhead *et al.* (1988) and Kulkarni (1989). Sources of bias in the bispectrum are evaluated in Pehlemann *et al.* (1992).

Aperture Masking Example

Let us consider an example from aperture masking. Two simple implementations of aperture masking are illustrated in Figure 13.5. The top series of panels document the use of the simplest mask possible, one with only two holes. The first panel shows the aperture mask being used, while the middle panel displays the corresponding "image" at the focal plane of the telescope. One sees a fringe pattern as expected from a simple Young's experiment, with fringes running in the same direction as the hole-separation vector. The overall size of the fringe envelope is determined by the diffraction patterns of the individual holes. The two-dimensional power spectrum of the image fringes can be used to determine the exact fringe frequency and fringe amplitude, as can be seen in the right-most panel. The spot in the center is the DC-term, and is proportional to the square of the total flux in the image frame. The spots to the right and left correspond to the fringe frequency and the spatial frequency value for them is proportional to the hole-separation. Since the power spectrum of a real function is inversion-symmetric, there is equal fringe power at both positive and negative spatial frequencies. Note the finite sizes of the spots in the power spectrum; this results from the finite size of the holes, reflecting the multiple baselines that stretch from one hole to the other. Note that the geometry of the power spectrum is directly related to the autocorrelation of the pupil mask via the Convolution Theorem (see Chapter 2, Section 2.5).

The bottom series of panels shows the next most complicated arrangement of holes for an aperture mask; one hole has been added to the first mask. One can clearly see in the middle pattern the effect of the additional hole. Now three baselines exist and thus three intersecting fringe patterns form, adding constructively and deconstructively in a pattern of spots. One can extract the amplitudes and exact spatial frequencies of the three fringe patterns by taking the power spectrum, which appears to the right. The original left-right baseline is still there, but now one can see the two new diagonal baselines. The closure phase can be found by Fourier transforming each image created through such a mask, and the Fourier phases summed from the appropriate spatial frequency bins. The location of the origin (phase center) during the Fourier transform does affect the individual phases determined for each baselines. However, its straightforward to prove that the closure phase is not sensitive to the choice of origin. This is equivalent to saying that the closure phase is independent of image translation. Indeed, for any set of three telescopes, it would be impossible to distinguish between an image translation or atmospheric phase disturbances.

An example of closure-phase analysis has been included in Figure 13.6 from actual data using an aperture mask on the Keck Telescope (see Section 13.3.5). The top panel shows the phases measured on three separate baselines for 100 short-exposure images on a point-source calibrator. Except for the shortest baseline (filled circles) which somewhat cluster

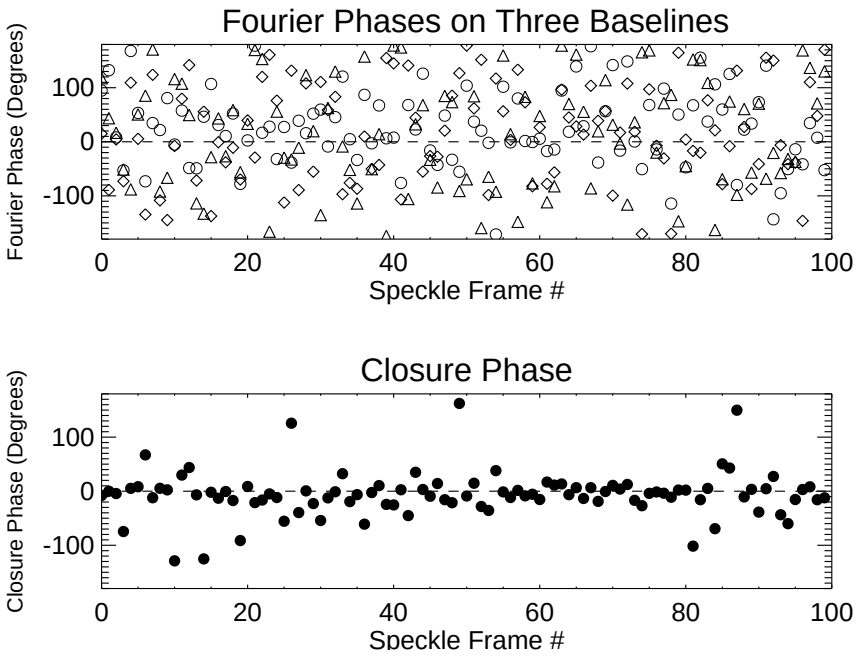

Figure 13.6: This figure illustrates the utility of closure phase averaging from real data. The top panel shows the Fourier phases of three fringe patterns, corresponding to a closed triangle of three baselines. The observed phases are marked by three different plot symbols for 100 separate frames. The bottom panel shows the closure-phase signal resulting from summing the above phases around the baseline triangle.

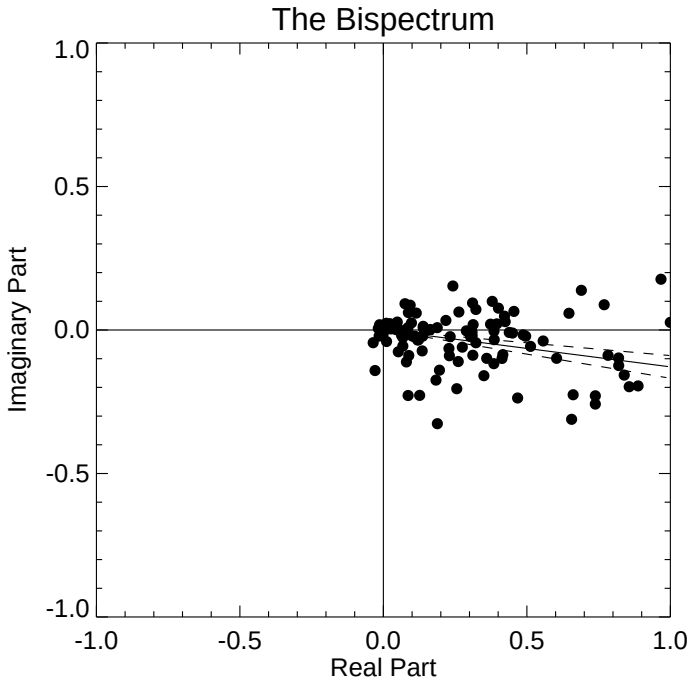

Figure 13.7: This figure shows the 100 bispectrum measurements and the vector average.

around 0°, the individual Fourier phases are pretty evenly spread between −180° and +180°. However, when the phases are summed in the appropriate way, this closure-phase quantity has much less dispersion than the individual phase measurements and is equal to about zero degrees. Using proper weighting, the uncertainty in the above measurement of the closure phase can be reduced to only ∼2° for just 100 frames; such accurate closure phases are essential for reliable image reconstructions of complicated sources. As discussed above, the best way to determine the closure phase is to average the bispectrum in the complex plane, as shown in Figure 13.7.

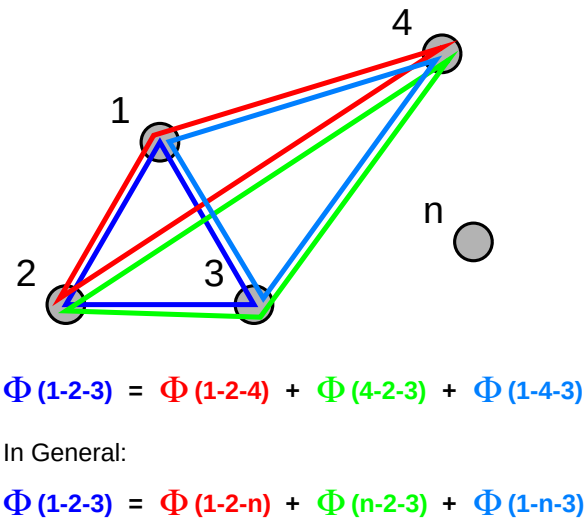

Figure 13.8: This figure illustrates important closure-phase relations.

13.2.4 Closure Phase Relations

For N telescopes, there are "N choose 3,"

$$\binom{N}{3} = \frac{(N)(N-1)(N-2)}{(3)(2)},$$

possible closing triangles. However, there are only

$$\binom{N}{2} = \frac{(N)(N-1)}{2}$$

independent Fourier phases; clearly not all the closure phases can be independent. Figure 13.8 illustrates how any given closure phase can be expressed as a sum of three others. The number of *independent* closure phases is only

$$\binom{N-1}{2} = \frac{(N-1)(N-2)}{2},$$

equivalent to holding one telescope fixed and forming all possible triangles with that telescope. The number of independent closure phases is always less than the number of phases

Table 13.1: Phase information contained in the closure phases alone

Number of Telescopes	Number of Fourier Phases	Number of Closing Triangles	Number of Independent Closure Phases	Percentage of Phase Information
3	3	1	1	33%
7	21	35	15	71%
21	210	1330	190	90%
27	351	2925	325	93%
50	1225	19600	1176	96%

one would like to determine, but the *percent* of phase information retained by the closure phases improves as the number of telescopes in the array increases. Table 13.1 lists the number of Fourier phases, closing triangles, independent closure phases, and recovered percentage of phase information for telescope arrays of 3 to 50 elements. For example, approximately 90% of the phase information is recovered with a 21-telescope interferometric array (e.g., Readhead *et al.* 1988). This phase information can be coupled with other image constraints (e.g., finite size and positivity) to reconstruct the source brightness distribution (see Section 13.3).

13.2.5 Simple Cases

Equal Binary

Since the closure phases are independent of the phase center, one can strategically place the origin in order to more easily determine the Fourier phases for a given brightness distribution. For example, consider the equal binary system depicted in Figure 13.9. The complex visibility can be easily written by choosing the origin midway between the two components. If $\mathbf{u}$ is the baseline vector and ρ is the separation vector of the binary, we have

$$\begin{aligned} V &= 0.5\left[\exp\left(-2\pi\mathbf{u}\cdot\frac{\rho}{2}\right)+\exp\left(2\pi\mathbf{u}\cdot\frac{\rho}{2}\right)\right] \\ &= \cos\left(2\pi\mathbf{u}\cdot\frac{\rho}{2}\right) \end{aligned} \tag{13.16}$$

Note the abrupt phase jump when the visibility amplitude goes through a null. These discontinuities are smoothed out when the two components are not precisely equal.

But what about the closure phases? Since a closure phase is simply a sum of three phases, we can immediately see that all the closure phases must be either 0° or 180°. In fact, this is true not just for equal binaries, but *any point-symmetric brightness distribution*. This is easily proven: by placing the origin (phase center) at the location of point-symmetry, then we can make the imaginary part of the Fourier transform disappear (i.e., all odd basis functions must be zero). Hence, the phases of *all* Fourier components must be either 0° or 180°.

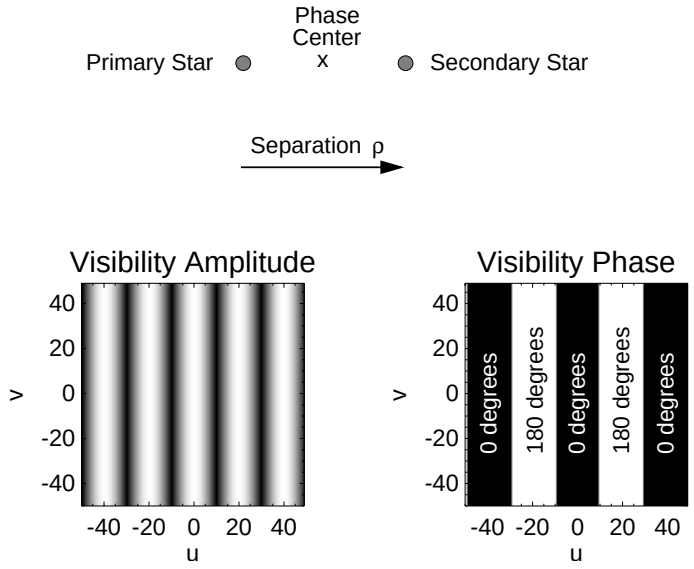

Figure 13.9: This figure shows the complex visibility for an equal binary system. With the above choice for the phase center, the Fourier phases can be represented simply. Notice the abrupt phase jumps when visibility amplitude goes through a null.

For an equal binary then, we would expect to see abrupt closure-phase jumps between 0° and 180° if one of the baselines traverses a null in the visibility pattern. This indeed has been observed with COAST (Baldwin *et al.*, 1996) and with the NPOI (Benson *et al.*, 1997). One can determine the binary separation (and brightness ratio) from the closure-phase information alone.

Faint Hotspot on Stellar Surface

In Figure 13.10, a more complicated example is illustrated, a star with a hotspot. This can be thought of as unequal binary with one of the components being resolved. For closing triangles with all short baselines (compared to that needed to resolve the star itself), the flux from the star itself dominates the visibility measurement. Hence, the system looks mostly centro-symmetric (like a round star), and we expect closure phases to be small. For triangles containing all long baselines, the star itself is mostly resolved and the hotspot dominates the appearance. In this limiting case as well, the closure phases should all be zero. This illustrates how an interferometer acts as a spatial filter, allowing only image details of certain spatial scales to be detected.

It is only at intermediate baselines, when the star itself is partially resolved, that non-zero (and non-180°) values of the closure phases are expected. Hence, we see the importance of having a variety of closing triangles available, since only some of them will contain useful information about the source structure. For instance, without intermediate-sized closing

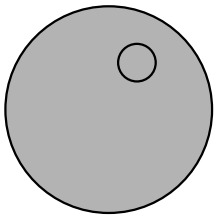

At low resolution, stellar disk dominates: Point-symmetric.

At highest resolution, stellar disk is resolved. Hotspot by itself is also Point-symmetric.

Figure 13.10: This illustrates the behavior of closure phases for a source consisting of a star with a hotspot. At both high and low spatial resolutions, the closure phases should be near zero. Only at intermediate baselines will the closure phases have significant non-zero values.

triangles, we would know the size of the star and reveal the presence of a hotspot, but we would only weakly constrain the hotspots position on the stellar surface. Very convincing measurements of non-zero/180° closure phases (or more simply, imaginary bispectral components) can be found in Tuthill (1994) and associated papers, establishing the presence of hotspots on a number of evolved giants and supergiants.

13.2.6 Summary

There are a few important points to remember from this section.

- The bispectrum is always real for sources with *point symmetry*. That is, the closure phases are all 0° or 180°.
- Closure phases are not sensitive to an overall translation of image. A translation is indistinguishable from atmospheric phase delays for any given closing triangle.
- The closure phases, or bispectrum, are independent of *telescope-specific* phase errors. Non-zero closure phases from a point source can result from having non-closing triangles and phase delays after beam combination.

13.3 Imaging

While modeling visibility and closure-phase data with simple models is useful, one would like to make an image unbiased by theoretical expectations. With a large number of measurements, images of arbitrary complexity should be attainable using optical/infrared interferometers and reliable closure-phase measurements. This section will discuss strategies currently employed, based on the techniques of Very Long Baseline Interferometry (VLBI) in the radio.

13.3.1 Converting Bispectrum to Complex Visibilities

In order to make an image from an interferometer, one needs estimates of the complex visibilities over a large portion of the (u, v) plane, both the amplitudes *and* phases. Unfortunately, there are not as many independent closure phases as there are Fourier phases (for non-redundant arrays), hence there is not a unique mapping from closure phases to Fourier phases. This would seem to make inverting the closure phases into the original Fourier phases a mathematical impossibility.

Baseline Redundancy—Baseline Bootstrapping

One way to get around this problem is to introduce baseline redundancy into the interferometric array. Figure 13.11 shows a simple four-element, linear, redundant array. Baselines connecting telescopes 1–2, 2–3 and 3–4 are all identical. Hence, the number of independent Fourier Phases is reduced from 6 to only 3. We can always assign the shortest baseline Fourier phase to be zero, since this encodes the position information which can not be extracted from the closure-phase data anyway. Consider the arrows drawn on Figure 13.11; these represent some of the baselines and closure triangles possible to have in this geometry. The Fourier phase of baseline 1–3 can be determined from the Fourier phases on the identical baselines 1–2 and 2–3 (which are equal and set to zero) and the closure phase 1–2–3. Now that we have the phase for baseline 1–3, we can determine the Fourier phase for baseline 1–4, by using the closure phase 1–3–4 and the (now) known phases for baselines 1–3 (just deduced) and 3–4 (same as 1–2 because of baseline redundancy). This process can be repeated to directly solve for all the Fourier phases given only the closure phases and setting the short baseline to zero phase.

While this process has found application for direct image reconstruction based on speckle interferometry (e.g., Cruzalebes *et al.* 1996; Koresko 1993), there are a number of problems with this approach. Because the short baseline phases must be determined first in order to "spiral-out" and solve for longer baselines, the long-baseline phases have much higher

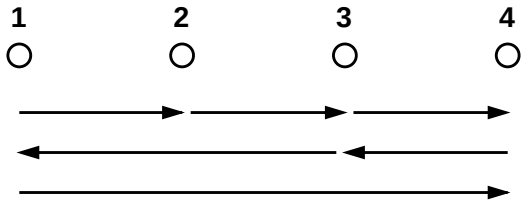

Figure 13.11: This is an example of a redundant four-element array geometry. Notice how baselines 1–2, 2–3, and 3–4 are identical; this allows the phase on baseline 1–3 to be determined using the closure phase 1–2–3 and only a single Fourier phase 1–2.

noise. This poor noise propagation can be improved by regularizing the inversion process, taking into account the noise and solving for a best fit. Simple regularization methods fail to properly handle phase wrapping and make this process vulnerable to significant errors unless handled with relatively high numerical sophistication.

Redundant arrays result in significantly poorer sampling in the Fourier plane, (u, v) coverage, than non-redundant alternatives when there are only a few telescopes. This would argue against deploying interferometric elements in such a manner. Interestingly however, baseline bootstrapping methods for allowing fringe tracking on long baselines with low-visibility amplitudes may necessitate partially redundant arrays for future sensitive optical/infrared interferometers (see Chapter 14). Under these conditions, the ability to directly solve for the Fourier phases from the closure phases may be quite valuable.

Applying Image Constraints

Another way of determining the Fourier phases from a limited number of closure phases is to apply image constraints. For instance, brightness distributions are always non-negative and generally have a finite extent. This is especially true in the infrared where thermal emission is almost always quite compact. These constraints introduce correlations in the Fourier amplitudes and phases, and essentially remove degrees of freedom from our inversion problem. The rest of this section will explore this strategy for image reconstruction using closure phases.

13.3.2 Imaging Goals

The goals of an image-reconstruction procedure can be stated quite simply: find an image which fits both the visibility amplitudes and closure phases within experimental uncertainties. However in practice, there are an infinite number of candidate images which satisfy this criterion, because interferometric data are always incomplete and noisy. Furthermore, the closure phases can not be used to unambiguously arrive at Fourier phase estimates as stated above, even under ideal noise-free conditions.

Additional constraints are imposed to "select" an image as the best-estimate of the true brightness distribution. Some of the most common ones are described below.

- Limited Field-of-View. This constraint is always imposed in aperture synthesis imaging, even for a fully-phased array (e.g., VLA). Limiting the field-of-view introduces correlations in the complex visibility in the (u, v) plane. This is a consequence of the Convolution Theorem (Chapter 2, Section 2.5), where a multiplication in image-space is equivalent to a convolution in the corresponding Fourier-space.

- Positive-Definite. Since brightness distributions can not be negative, this is a sensible constraint. While clearly limiting the range of "allowed" complex visibilities, there are

few obvious, intuitive effects in the Fourier-plane; one is that the visibility amplitude is maximum at zero spatial frequency. The Maximum Entropy Method (see Section 13.3.3) naturally incorporates this constraint.

- "Smoothness." The Maximum Entropy Method, for instance, selects the "smoothest" image consistent with the data.
- *A Priori* Information. One can incorporate previously known information to constrain the possible image reconstructions. For instance, a low-resolution image may be available from a single-dish telescope. Another commonly encountered example is a point source embedded in a nebulosity; one might want the reconstruction algorithm to take into account that the source at the center is point-like from theoretical arguments.

13.3.3 "Standard" Aperture Synthesis Imaging

For a phased interferometric array (e.g., the VLA), one can use a number of aperture synthesis techniques to produce an estimate of an image based on sparsely sampled Fourier components. These procedures basically remove artifacts, i.e. sidelobes, of the interferometer's point-source response arising from uneven sampling of the (u, v) plane. These procedures do not incorporate closure phases, but work by inverting the Fourier amplitudes and phases to make an image. A brief explanation of the most popular algorithms CLEAN and MEM follow with additional references for the interested reader. See Perley *et al.* (1986) for essays on these topics aimed at radio astronomers.

CLEAN

Originally described by Högbom (1974), CLEAN has been traditionally the most popular algorithm for image reconstruction in radio interferometry because it is both computationally efficient and intuitively understandable. Given a set of visibility amplitudes and phases over a finite region of the Fourier plane, the "true" image can be estimated by simply setting all other spatial frequencies to zero and taking the Fourier Transform. As one might expect, this process leads to a whole host of image artifacts, most damaging being positive and negative "sidelobes" resulting from non-complete coverage of the Fourier plane; we call this the "dirty map." The unevenly-filled Fourier plane can be thought of as a product of a completely-sampled Fourier plane (which we desire to determine) and a spatial frequency mask which is equal to 1 where we have data and 0 elsewhere. Since multiplication in Fourier space is identical to convolution in image space, we can take the Fourier transform of the spatial frequency mask to find this convolving function; we call this the "dirty beam." Now the image reconstruction problem can be recast as a "deconvolution" of the dirty map with the dirty beam.

The dirty map is CLEANed by subtracting the dirty beam (scaled to some fraction of the map peak) from the brightest spot in the dirty map. This removes sidelobe structure and artifacts from the dirty map. Repeating this process with dirty beams of ever decreasing amplitudes leads to a series of delta-functions which, when combined, fit the interferometric data. For visualization, this map of point sources is convolved with a Gaussian function whose full-width at half-maximum (FWHM) values are the same as the dirty beam; this removes high spatial resolution information beyond the classic "Rayleigh" criterion cutoff. One major weakness with CLEAN is that this smoothing changes the visibility amplitudes, hence the CLEANed image no longer strictly fits the interferometric data, especially the spatial frequency information near the diffraction limit. Another weakness is that CLEAN does not directly use the known uncertainties in the visibility data, and hence there is no natural method to weight the high signal-to-noise data more than the low signal-to-noise data during image reconstruction. Further discussion of various implementations of CLEAN can be found in Clark (1980), Schwab (1984), Cornwell (1983), and Chapter 7 of Perley *et al.* (1986) by T. Cornwell.

MEM

The maximum entropy method (MEM) makes better use of the highest spatial frequency information by finding the *smoothest* image consistent with the interferometric data. While enforcing positivity and conserving the total flux in the frame, "smoothness" is estimated here by a global scalar quantity S, the "entropy." If f_i is the fraction of the total flux in pixel i, then

$$S = -\sum_i f_i \ln \frac{f_i}{I_i} \tag{13.17}$$

after the thermodynamic quantity; I_i is known as the *image prior* and must be specified by the user. The MEM map f_i will tend toward I_i when there are little (or noisy) data to constrain the fit. Often I_i is assumed to be a uniformly bright background, however one can use other image priors if additional information is available, such as the overall size of the source which may be known from previous observations.

Mathematically, MEM solves the multi-dimensional (N=number of pixels) constrained minimization problem which only recently has become computationally realizable on desktop computers. Maintaining an adequate fit to the data ($\chi^2 \sim$ number of degrees of freedom), MEM reconstructs an image with maximum S. MEM image reconstructions always contain some spatial frequency information beyond the diffraction limit in order to keep the image as "smooth" as possible consistent with the data. Because of this, images typically have maximum spatial resolution a few times smaller than the typical Rayleigh-type resolution encountered with CLEAN ("super-resolution"). Further discussions of MEM and related Bayesian methods can be found in Pina and Puetter (1992), Narayan and Nityananda (1986), Skilling and Bryan (1984), Gull and Skilling (1984), and Sivia (1987).

Unfortunately, MEM images also suffer from some characteristic artifacts and biases. Photometry of MEM-deconvolved images is necessarily biased because of the positivity constraint; any noise or uncertainty in the imaging appears in the background of the reconstruction instead of the source, systematically lowering the estimated fluxes of compact sources. Also, fields containing a point source embedded in extended emission often show structure reminiscent of Airy rings, the location of the rings being influenced by the wavelength of the observation and not inherent to the astrophysical source. Fortunately, these imaging artifacts are greatly alleviated for asymmetric structures, when closure phases and not the visibility amplitudes play a dominant role in shaping the reconstructed morphology.

13.3.4 Including Closure Phase Information

The above algorithms were designed to use Fourier amplitudes and phases, not closure phases. Early image reconstruction algorithms incorporated closure-phase information by using an iterative scheme (Thompson *et al.* 1986; Readhead and Wilkinson 1978). The following steps summarize this process:

1. Start with a "phase model" based on either prior information or setting all phases to zero.
2. Determine candidate phases by using some values from the "phase model" and enforcing all the (self-consistent) closure-phase relations (see Section 13.2.4).
3. Using CLEAN or MEM, perform aperture synthesis mapping on the given visibilities and candidate phases. At this stage, image constraints such a positivity and/or finite support are applied.
4. Use this image as a basis for a new "phase model."
5. Go to step 2 and repeat until the process converges to a stable image solution.

"Self-Calibration"

Cornwell and Wilkinson (1981) introduced a modification of the above scheme by explicitly solving for the telescope-specific errors as part of the reconstruction step. Hence the measured (corrupted) Fourier phases are fit using a combination of intrinsic phases (which are used for imaging using CLEAN/MEM) plus telescope phase errors. In this scheme, the closure phases are not explicitly fit, but rather are conserved in the procedure since varying telescope-specific errors can not change any of the closure phases. Figure 13.12 shows a flow diagram for this procedure, and requires thoughtful consideration in order to fully understand the power and elegance of "self-cal."

Self-calibration works remarkably well for large number of telescopes, but requires reasonably high signal-to-noise ratio (SNR$\gtrsim$5) in the measured complex visibilities. Once the

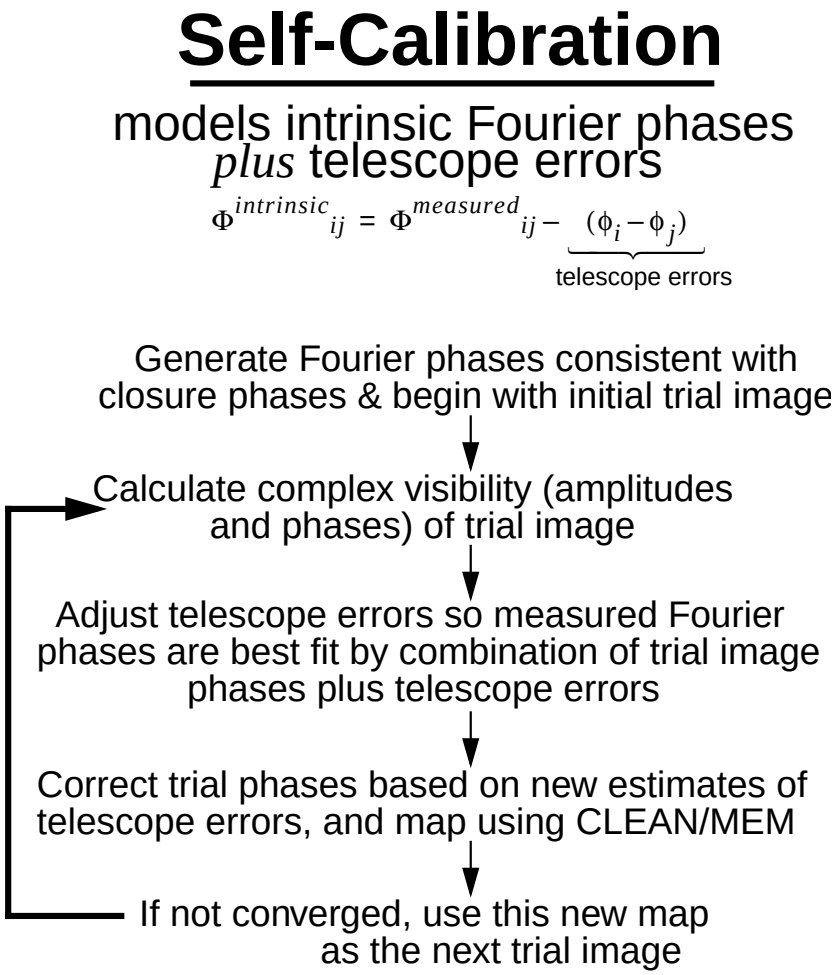

Figure 13.12: This is a flow diagram for a incorporating closure-phase information into CLEAN/MEM aperture synthesis imaging algorithms based on the "self-calibration" procedure of Cornwell and Wilkinson (1981).

signal-to-noise ratio decreases below this point, the method completely fails. This conceptualization, while useful for radio interferometry, fails for optical/infrared interferometry where the good observables are the closure phases themselves, not corrupted Fourier phases. This is because the time-scale for phase variations in the optical/infrared is much less than a second, as opposed to minutes/hours in the radio.

13.3.5 Imaging Results from Keck Aperture Masking

Detailed images of dusty circumstellar envelopes have been made by performing aperture masking interferometry on the Keck-I telescope at near-IR wavelengths. Both non-redundant and partially-redundant array geometries have been used with success. The methodology was as follows. A set of visibility amplitudes and closure phases was obtained from a series of 100 speckle frames. These data were calibrated by using an equal number of frames taken on a nearby point-source calibrator. A set of Fourier phases consistent with the measured closure phases (to within noise) was then generated using an iterative relaxation technique (Monnier 1999), avoiding phase-wrapping problems of Singular Value Decomposition methods. This allowed the data to be represented in terms of visibility amplitudes and "corrupted" Fourier phases. After data conversion to a VLBI data format, the self-calibration/MEM routines of Sivia (1987) were used to produce diffraction-limited images. Results from this experiment as well as details regarding observing methodology and mask geometries can be found in various publications (e.g., Tuthill *et al.* 1998; Monnier 1999; Monnier *et al.* 1999; Tuthill *et al.* 1999; Tuthill *et al.* 2000).

IRC +10216 and WR 104

In this section I present images of dust shells around IRC +10216 and WR 104. To illustrate the importance of phase information to accurately reconstruct images of complicated objects, I have included MEM reconstructions using no phase information as well as reconstructions taking advantage of the measured closure phases. Figure 13.13 contains these results.

Spurious symmetrization is observed in the images with no phase information; this is because the phases were set equal to zero for definiteness. This enforced point-symmetry and explains the symmetry observed in the upper panels. Note that the dust shells around these stars do not conform to the spherically-symmetric, uniform-outflowing dust density distributions which were theoretically expected. These dust shells have been fit for many years using spherically-symmetric dust shell models, because insufficient data existed to make maps free of theoretical bias. Imaging of astrophysical objects is quite important for confirming theoretical ideas, and these examples showcase the potential of long-baseline interferometry to produce images of complicated environments using closure-phase imaging techniques when arrays with sufficient numbers of telescopes come into service.

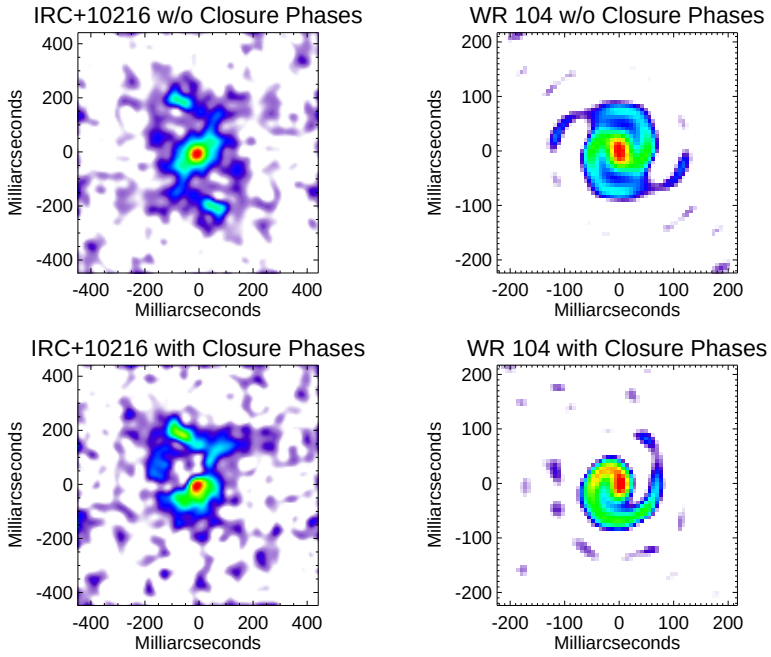

Figure 13.13: (*top panels*) These panels show K-band reconstructions of IRC +10216 and WR 104 with no phase information. (*bottom panels*) These panels show the maps when closure-phase information is taken into account.

13.4 Outstanding Issues

There are a number of problems with existing software being used for image reconstruction by long-baseline optical/infrared interferometry groups. The adoption of phase-referencing techniques by the VLA and VLBA has allowed direct Fourier inversion of the interferometry data, using CLEAN or MEM, without requiring a self-calibration step. For this reason (I believe), scant software or theoretical progress has been made in the last 10 years. Disappointingly, the immense potential of the exponential increase in computing power has remained unrealized.

13.4.1 Overview of Problems

Here is an incomplete list of some of the outstanding problems with the current status of image reconstruction software for optical/infrared long-baseline interferometry data:

- There is no agreed data storage format for optical/infrared interferometry data. Standard radio formats (UVFITS) record complex visibilities rather than the bispectrum or closure phases. Some have suggested a NASA-derived standard be adopted, since IPAC will presumably need to archive data from upcoming interferometry projects (e.g., SIM and the Keck Interferometer). Others believe an extension of FITS, within the AIPS++ paradigm, may be better.

- Algorithms should fit directly to the good observables, i.e. the closure phases (bispectrum) and power spectra. This is straightforward, although more computationally expensive. The "self-cal" concept of fitting to the telescope errors breaks down, since the atmosphere is cycling the phase many times every second.
- Fits based on the scalar χ^2 have baseline-dependent residuals when used with most regularization schemes. Use of multi-resolution approaches or more sophisticated "goodness-of-fit" criteria should be attempted.
- A point source embedded in extended nebulosity is often encountered, yet common image reconstruction algorithms (e.g., MEM) introduce bad artifacts under these conditions ("ringing"). Use of this type of *a priori* information should be included in new algorithms.
- New generation of interferometers have from three to seven elements (usually three). This will result in quite uneven Fourier coverage, and new strategies, both for planning observations and reconstructing images, will likely be required if imaging of moderately complex sources are desired.

Note that solving the above problems will also extend the usefulness of speckle interferometry, for most users of these techniques are not optimally using their data. In addition, there may be advantages of combining aperture-masking with new adaptive optics systems (e.g., Haniff and Wilson 1994).

13.4.2 New Possibilities

Before concluding this section, I want to mention some interesting new techniques which show promise for solving some of the above problems. While efforts to reconstruct images based on the bispectrum alone have a relatively long history (e.g., Weigelt 1977), only recently have these techniques seen success imaging complicated environments (Hofmann and Weigelt 1993; Weigelt *et al.* 1998). Recent work applied to mm-wave interferometry, which has similar atmospheric phase issues, can be found in Katagiri *et al.* (1997). Some of the artifacts of MEM and CLEAN could be avoided by developing new aperture synthesis approaches, based on wavelets (Starck *et al.* 1994), pixon-based methods (Pina and Puetter 1993; Yahil 1999), or WIPE (Lannes *et al.* 1997). For the serious reader, I recommend the series of difficult but interesting papers relating closure-phase imaging to algebraic graph theory (Lannes 1990; Lannes *et al.* 1997; Lannes 1998b; Lannes 1998a); the power of these ideas are surely underutilized.

13.5 Summary of Important Points

- Closure phases and closure amplitudes are insensitive to *telescope-specific* errors such as atmospheric phase delays.
- Closure phases and closure amplitudes *can not* be used to calibrate *baseline-dependent* problems.
- All point-symmetric objects (including disks) yield closure phases of either 0° or 180°, i.e. the bispectrum is entirely *real*. Hence, closure phases act as strong probes of asymmetric structure, even when source structure can not be fully resolved.
- Software and theoretical work is absolutely necessary for optimal imaging with the current generation of long baseline interferometers.
- Despite the total scrambling of Fourier phases by a turbulent atmosphere, the use of closure phases and image constraints allow nearly complete recovery of all phase information.

Acknowledgments

I would like to thank Chris Haniff for helpful discussions.

References

J.E. Baldwin, C.A. Haniff, C.D. Mackay, and P.J. Warner, "Closure phase in high-resolution optical imaging," Nature **320**, 595–597 (1986).

J.E. Baldwin, M.G. Beckett, R.C. Boysen, D. Burns, D.F. Buscher, G.C. Cox, C.A. Haniff, C.D. Mackay, N.S. Nightingale, J. Rogers, P.A.G. Scheuer, T.R. Scott, P.G. Tuthill, P.J. Warner, D.M.A. Wilson, and R.W. Wilson, "The first images from an optical aperture synthesis array: mapping of Capella with COAST at two epochs." Astron. Astrophys. **306**, L13–L16 (1996).

J.A. Benson, D.J. Hutter, N.M. Elias II, P.F. Bowers, K.J. Johnston, A.R. Hajian, J.T. Armstrong, D. Mozurkewich, T.A. Pauls, L.J. Rickard, C.A. Hummel, N.M. White, D. Black, and C.S. Denison, "Multichannel optical aperture synthesis imaging of Zeta 1 Ursae Majoris with the navy prototype optical interferometer." Astron. J. **114**, 1221–1226 (1997).

M. Bester, W.C. Danchi, C.G. Degiacomi, L.J. Greenhill, and C.H. Townes, "Atmospheric fluctuations - empirical structure functions and projected performance of future instruments," Astrophys. J. **392**, 357–374 (1992).

M. Born and E. Wolf, *Principles of Optics*, 7 (expanded) edn. (Cambridge, UK: Cambridge University Press, 1999).

B.G. Clark, "An efficient implementation of the algorithm 'CLEAN'," Astron. Astrophys. **89**, 377–378 (1980).

M.M. Colavita, J.K. Wallace, B.E. Hines, Y. Gursel, F. Malbet, D.L. Palmer, X.P. Pan, M. Shao, J.W. Yu, A.F. Boden, P.J. Dumont, J. Gubler, C.D. Koresko, S.R. Kulkarni, B.F. Lane, D.W. Mobley, and G.T. Van Belle, "The Palomar Testbed Interferometer," Astrophys. J. **510**, 505–521 (1999).

T.J. Cornwell, "A method of stabilizing the clean algorithm," Astron. Astrophys. **121**, 281–285 (1983).

T.J. Cornwell and P.N. Wilkinson, "A new method for making maps with unstable radio interferometers," Mon. Not. R. Astron. Soc. **196**, 1067–1086 (1981).

P. Cruzalebes, E. Tessier, B. Lopez, A. Eckart, and D. Tiphene, "Diffraction limited near-infrared imaging of the Red Rectangle by bispectral analysis." Astron. Astrophys. Sup. Ser. **116**, 597–610 (1996).

D.T. Gavel, H.W. Friedman, and S.S. Olivier, "Wide-baseline optical interferometry with laser guide stars," in *Astronomical Interferometry*, R.D. Reasenberg, ed., Proc. SPIE **3350**, 793–799 (1998).

S.F. Gull and J. Skilling, "The maximum entropy method," in *Indirect Imaging*, J.A. Roberts, ed., (Cambridge University Press: Cambridge, UK, 1984), pp. 267–279.

C.A. Haniff, D.F. Buscher, J.C. Christou, and S.T. Ridgway, "Synthetic aperture imaging at infrared wavelengths," Mon. Not. R. Astron. Soc. **241**, 51P–56P (1989).

C.A. Haniff, C.D. Mackay, D.J. Titterington, D. Sivia, and J.E. Baldwin, "The first images from optical aperture synthesis," Nature **328**, 694–696 (1987).

C.A. Haniff and R.W. Wilson, "Closure-phase imaging with partial adaptive correction," Pub. Astron. Soc. Pac. **106**, 1003–1014 (1994).

K.-H. Hofmann and G. Weigelt, "Iterative image reconstruction from the bispectrum," Astron. Astrophys. **278**, 328–339 (1993).

J.A. Högbom, "Aperture synthesis with a non-regular distribution of interferometer baselines." Astron. Astrophys. Sup. Ser. **15**, 417–426 (1974).

R.C. Jennison, "A phase sensitive interferometer technique for the measurement of the Fourier transforms of spatial brightness distributions of small angular extent," Mon. Not. R. Astron. Soc. **118**, 276–284 (1958).

R.C. Jennison, "The Michelson stellar interferometer: a phase sensitive variation of the optical instrument," Proc. Phys. Soc. **78**, 596–599 (1961).

S. Katagiri, K.-I. Morita, N. Kawaguchi, and M. Hayakawa, "An imaging algorithm using the bispectrum in radio interferometry," Pub. Astron. Soc. Japan **49**, 123–129 (1997).

C. Koresko, *The Early Evolution of Binary Stars*, Ph.D. thesis, Cornell University (1993).

S.R. Kulkarni, "Self-noise in interferometers – radio and infrared," Astron. J. **98**, 1112–1130 (1989).

A. Lannes, "Remarkable algebraic structures of phase-closure imaging and their algorithmic implications in aperture synthesis," J. Opt. Soc. Am. A **7**, 500–512 (1990).

A. Lannes, "Imaging capabilities of weak-phase interferometric devices," in *Astronomical Interferometry*, R.D. Reasenberg, ed., Proc. SPIE **3350**, 996–1003 (1998a).

A. Lannes, "Weak-phase imaging in optical interferometry," J. Opt. Soc. Am. A **15**, 811–824 (1998b).

A. Lannes, E. Anterrieu, and P. Marechal, "CLEAN and WIPE," Astron. Astrophys. Sup. Ser. **123**, 183–198 (1997).

J.D. Monnier, P.G. Tuthill, B. Lopez, P. Cruzalebes, W.C. Danchi, and C.A. Haniff, "The last gasps of VY CMa: Aperture synthesis and adaptive optics imaging," Astrophys. J. **512**, 351–361 (1999).

J.D. Monnier, *Infrared Interferometry and Spectroscopy of Circumstellar Envelopes*, Ph.D. thesis, University of California at Berkeley (1999).

R. Narayan and R. Nityananda, "Maximum entropy image restoration in astronomy," Ann. Rev. Astron. Astrop. **24**, 127–170 (1986).

E. Pehlemann, K.-H. Hofmann, and G. Weigelt, "Photon bias compensation in triple correlation imaging and observation of R 136," Astron. Astrophys. **256**, 701–714 (1992).

R.A. Perley, F.R. Schwab, and A.H. Bridle, in *Synthesis Imaging: Course Notes from an NRAO Summer School*, NRAO Workshop **13** (Green Bank, WV: National Radio Astronomy Observatory, 1986).

R.K. Pina and R.C. Puetter, "Incorporation of spatial information in Bayesian image reconstruction: The maximum residual likelihood criterion," Pub. Astron. Soc. Pac. **104**, 1096–1103 (1992).

R.K. Pina and R.C. Puetter, "Bayesian image reconstruction - the pixon and optimal image modeling," Pub. Astron. Soc. Pac. **105**, 630–637 (1993).

A.C.S. Readhead and P.N. Wilkinson, "The mapping of compact radio sources from VLBI data," Astrophys. J. **223**, 25–36 (1978).

A.C.S. Readhead, T.S. Nakajima, T.J. Pearson, G. Neugebauer, J.B. Oke, and W.L.W. Sargent, "Diffraction-limited imaging with ground-based optical telescopes," Astron. J. **95**, 1278–1296 (1988).

F. Roddier, "Triple correlation as a phase closure technique," Opt. Comm. **60**, 145–148 (1986).

D.H. Rogstad, "A technique for measuring visibility phase with an optical interferometer in the presence of atmospheric seeing," Appl. Opt. **7**, 585–588 (1968).

F.R. Schwab, "Relaxing the isoplanatism assumption in self-calibration; applications to low-frequency radio interferometry," Astron. J. **89**, 1076–1081 (1984).

M. Shao and M.M. Colavita, "Potential of long-baseline infrared interferometry for narrow-angle astrometry," Astron. Astrophys. **262**, 353–358 (1992).

D. Sivia, *Phase Extension Methods*, Ph.D. thesis, Cambridge University, UK (1987).

J. Skilling and R.K. Bryan, "Maximum entropy image reconstruction: General algorithm," Mon. Not. R. Astron. Soc. **211**, 111–124 (1984).

Jean-Luc Starck, Albert Bijaoui, Bruno Lopez, and Christian Perrier, "Image reconstruction by the wavelet transform applied to aperture synthesis," Astron. Astrophys. **283**, 349–360 (1994).

A. R. Thompson, J. M. Moran, and G. W. Swenson, Jr., *Interferometry and synthesis in radio astronomy* (New York: Wiley-Interscience, 1986).

P. G. Tuthill, *Imaging Stars Through the Atmosphere*, Ph.D. thesis, University of Cambridge, England (1994).

P. G. Tuthill, J. D. Monnier, and W. C. Danchi, "Imaging of stellar disks and mass-loss envelopes in evolved stars," in *Asymptotic Giant Branch Stars*, A. Lebre, T. Le Bertre and C. Waelkens, eds., IAU Symposia **191**, 331–336 (1998).

P. G. Tuthill, J. D. Monnier, and W. C. Danchi, "A dusty pinwheel nebula around the massive star WR 104." Nature **398**, 487–489 (1999).

P. G. Tuthill, J. D. Monnier, W. C. Danchi, E. Wishnow, and C. A. Haniff, "Michelson interferometry with the Keck-I telescope," Pub. Astron. Soc. Pac. **112**, 555–565 (2000).

F. Vakili, D. Mourard, D. Bonneau, F. Morand, and P. Stee, "Subtle structures in the wind of P Cygni." Astron. Astrophys. **323**, 183–188 (1997).

G. Weigelt, Y. Balega, T. Bloecker, A. J. Fleischer, R. Osterbart, and J. M. Winters, "76 mas speckle-masking interferometry of IRC+10216 with the SAO 6m telescope: Evidence for a clumpy shell structure," Astron. Astrophys. **333**, L51–L54 (1998).

G. P. Weigelt, "Modified astronomical speckle interferometry 'speckle masking'," Opt. Comm. **21**, 55–59 (1977).

M. C. Wiedner, *Atmospheric water vapour and astronomical millimetre interferometry*, Ph.D. thesis, University of Cambridge, United Kingdom (1998).

G. Woan and P.J. Duffett-Smith, "Determination of closure phase in noisy conditions," Astron. Astrophys. **198**, 375–378 (1988).

A. Yahil, private communication (1999).